15 October 2002

ELSEVIER

Optics Communications 212 (2002) 127–138

OPTICS COMMUNICATIONS

www.elsevier.com/locate/optcom

Instabilities of lasers with moderately delayed optical feedback

Matthias Wolfrum*, Dmitry Turaev

Weierstrass Institute for Applied Analysis and Stochastics, Mohrenstr. 39, D-10117 Berlin, Germany

Received 12 February 2002; received in revised form 19 July 2002; accepted 29 July 2002

Abstract

We perform a bifurcation analysis of the Lang–Kobayashi system for a laser with delayed optical feedback in the situation of moderate delay times. Using scaling methods, we are able to calculate the primary bifurcations, leading to instability of the stationary lasing state. We classify different types of pulsations and identify a codimension two bifurcation of fold-Hopf interaction type as the organizing centre for the appearance of more complicated dynamics.

PACS: 42.44.Px; 42.65.Sf

Keywords: Laser with delayed optical feedback; Bifurcation analysis; Scaling methods

1. Introduction

Delayed optical feedback is one of the fundamental mechanisms, leading to instability and complicated dynamics in semiconductor lasers [1]. Optical feedback from an external mirror leads to delay times, which are large in comparison to the photon lifetime inside the cavity. This situation has been studied extensively, both numerically and in experiments, and shows a variety of complicated dynamical phenomena. For large distances of the mirror, there has been observed high dimensional chaos, so-called *low-frequency fluctuations* (see e.g. [2,3]). Other types of less irregular behaviour, called *regular pulse packages*, were observed for distances of only a few centimeters [4].

In contrast to that, the situation of smaller feedback time has received much less attention. It arises in integrated multi-section devices with a DFB laser section and a passive external cavity section which is only a few times larger than the active section. Devices of this type have been studied up to now mainly in the context of travelling-wave equations [13,14,20]. For such short feedback times, Petermann and Tager [8] discovered the possibility of high frequency pulsations (PT pulsations), caused by a beating between a mode and an antimode of the external cavity. This type of solutions has also been studied in [9–11].

In this paper, we will perform a bifurcation analysis for the Lang–Kobayashi system, restricted to the case of small and moderate feedback times. This will lead to a refined investigation of

* Corresponding author. Tel.: +49-30-2037-2486; fax: +49-30-204-4975.

E-mail addresses: wolfrum@wias-berlin.de (M. Wolfrum), turaev@wias-berlin.de (D. Turaev).

0030-4018/02/$ - see front matter
PII: S0030-4018(02)01824-2

how the stationary state of the laser without feedback undergoes changes, loses its stability, and with growing feedback gives rise to more complicated behaviour.

To this end, we first introduce an appropriately rescaled version of the Lang–Kobayashi model with strength an phase condition of the feedback signal as bifurcation parameters. In Section 2, we restate known results about stationary lasing states and their bifurcations [5–7] in this setting, derive a formula for the condition for PT pulsations and introduce the notion of mode degeneracy.

The importance of scaling techniques for a systematic understanding of the rather complicated characteristic equation of the delay system has been pointed out by Erneux in [12]. In Section 3, we use the smallness the ratio of feedback time and carrier lifetime to apply scaling techniques in order to obtain approximating solutions for the Hopf condition. In addition to the branch of bifurcations to PT pulsations, which has already been discussed in [12], we obtain a second type of solutions related to the DQS-pulsations, which were discussed in [14,15] for multi-section lasers. We investigate also the transition regime which matches these two branches of solutions and discuss the role of a codimension two bifurcation as an organizing centre for the appearance of more complicated dynamics. Finally, we point out the relevance of our asymptotic formulas for the bifurcation curves by comparison to numerical results for the full system.

The behaviour of a single moded laser under the influence of delayed optical feedback can be described by the Lang–Kobayashi rate equations

$$\frac{\mathrm{d}E}{\mathrm{d}t} = \frac{1}{2}\left(\mathscr{G}(N,|E(T)|^2) - \frac{1}{\tau_\mathrm{p}}\right)\cdot E(T) + \kappa \mathrm{e}^{-\mathrm{i}\omega_0\tau_\mathrm{f}}\cdot E(T-\tau_\mathrm{f}), \tag{1}$$

$$\frac{\mathrm{d}N}{\mathrm{d}T} = \mathrm{I} - \frac{N}{\tau_\mathrm{c}} - \mathrm{Re}[\mathscr{G}(N,|E(T)|^2)]\cdot|E(T)|^2, \tag{2}$$

for the field amplitude E and the carrier density N [16]. The lasing frequency ω_0 of the laser without feedback is used as the reference frequency, i.e., the actual field amplitude is given by $\frac{1}{2}(E(T)\mathrm{e}^{\mathrm{i}\omega_0 T} + \mathrm{c.c.})$. With I we denote the pumping current, and $\mathscr{G}(N,|E(T)|^2)$ is the complex gain function; $\tau_\mathrm{p}, \tau_\mathrm{c}, \tau_\mathrm{f}$ are photon lifetime, carrier lifetime, and feedback time. The feedback rate κ, has to be computed from the reflectivities, external losses, and the internal round-trip time (see [8]). Equations of this type have been shown to be able to describe a variety of different dynamical phenomena in good agreement with experimental data. Moreover, they can serve as a prototype model to understand the basic mechanisms leading to complicated dynamics in lasers with delayed optical feedback.

To the general system (1), (2) we introduce now some simplifications and rescalings. We want here to restrict our attention to situations, where the external round-trip time is not more than one order of magnitude bigger than the internal round-trip time. We use a rescaled time

$$t := \frac{T}{\tau_\mathrm{f}}.$$

Since we are not interested in high intensity effects, we neglect nonlinear gain saturation and linearize the complex gain function around the stationary lasing state ω_0, N_0 of the laser without feedback

$$\mathscr{G}(N,|E(T)|^2) - \frac{1}{\tau_\mathrm{p}} := G_N(1+\mathrm{i}\alpha)(N-N_0).$$

With the rescaling

$$N_\mathrm{res} := \frac{1}{2}\tau_\mathrm{f} G_N (N - N_0)$$

we have simplified the optical equation to

$$\frac{\mathrm{d}E(t)}{\mathrm{d}t} = (1+\mathrm{i}\alpha)N_\mathrm{res}\cdot E(t) + \eta \mathrm{e}^{-\mathrm{i}\phi}\cdot E(t-1), \tag{3}$$

with the effective feedback strength $\eta := \kappa\tau_\mathrm{f}$. The phase factor $\phi := \omega_0\tau_\mathrm{f}$ will be treated as an additional free parameter. This seems naturally to us, since already slight changes of τ_f change the phase condition from 0 to 2π.

We next introduce the new variables into the carrier equation, and additionally set

$$E_\mathrm{res} := \sqrt{\tau_\mathrm{c} G_\mathrm{N}} E.$$

This rescaling of E does not affect the linear equation (3). From this we obtain

$$\frac{\mathrm{d}N_\mathrm{res}(t)}{\mathrm{d}t} = \varepsilon\Big(J - N_\mathrm{res} - (N_\mathrm{res}+\nu)|E_\mathrm{res}|^2\Big) \tag{4}$$

with

$$\varepsilon := \frac{\tau_f}{\tau_c}, \tag{5}$$

$$J := \frac{\tau_f G_N}{2}(\tau_c I + N_0), \tag{6}$$

$$v := \frac{\tau_f}{2\tau_p}. \tag{7}$$

Note that $-v$ corresponds to the transparency density for the rescaled N.

In the sequel we will use only the rescaled equations (3), (4), omitting the subscripts for the rescaled variables N and E. The feedback parameters η and ϕ will be our primary bifurcation parameters. In addition we will make use of the fact that ε is small with respect to the other coefficients. This is still true for a length of the compound cavity of some millimeters.

2. The optical equation

2.1. Rotating waves and saddle-nodes

We start by recalling some basic facts about stationary lasing states for the Lang–Kobayashi system (compare e.g. [1,5,8]). Looking for rotating wave solutions of the form

$$E(t) = E_s e^{i\omega_s t}, \quad N(t) = N_s \tag{8}$$

in (3), one obtains the equation

$$i\omega_s = (1 + i\alpha)N_s + \eta e^{-i(\phi+\omega_s)}. \tag{9}$$

Splitting this into real and imaginary part gives the conditions

$$N_s = -\eta\cos(\phi + \omega_s), \tag{10}$$

$$\omega_s - \alpha N_s = -\eta\sin(\phi + \omega_s), \tag{11}$$

or equivalently, inserting (10) into (11),

$$\omega_s = -\eta(\alpha\cos(\phi + \omega_s) + \sin(\phi + \omega_s)). \tag{12}$$

The carrier equation (4) may be used to determine the intensity

$$|E_s|^2 = \frac{J - N_s}{N_s + v}, \tag{13}$$

but the carrier equation does not affect the conditions (10), (11) for N_s and ω_s. These rotating wave solutions are called in the literature *external cavity modes* (ECMs), and can be represented as points in the (ω, N)-plane. In our coordinates the origin in this plane corresponds to the stationary state of the laser without feedback. Then, for small feedback η, there is for all values of ϕ only one stable solution close to the origin, which for varying ϕ changes slightly its threshold density and optical frequency. For larger feedback, the number of solutions increases and some of them may be unstable.

Indeed, from (10), (11) it is clear that in the (ω, N)-plane all ECM solutions for fixed η are located on an ellipse around zero. This ellipse grows for increasing values of η. Changing only ϕ, all the solutions move along the ellipse (see [5]). These solutions are determined only by the optical equation (3), and we can use this equation also to some extend for a study of the stability and bifurcations of the stationary points.

If ω_s is a double root of (12), then we have a saddle-node bifurcation of rotating waves. To this end we differentiate (12) with respect to ω_s and obtain

$$1 = \eta(\alpha\sin(\phi + \omega_s) - \cos(\phi + \omega_s)). \tag{14}$$

Together with the conditions (10) and (11) this gives in the (ω, N)-plane the straight line (compare [5])

$$\omega_s = \alpha N_s - \frac{1 - N_s}{\alpha}. \tag{15}$$

Solutions above this line are always unstable, the solutions below may be stable or unstable. We want now to represent the condition for this bifurcation, as usually done in bifurcation theory, in the space of the main parameters η and ϕ. To this end, we first solve the transcendental equations (10), (11) for η and ϕ, obtaining

$$\eta = \sqrt{N^2 + (\omega - \alpha N)^2}, \tag{16}$$

$$\phi = \begin{cases} \arccos(-\frac{N}{\eta}) - \omega & \text{for} \quad \omega - \alpha N \geqslant 0, \\ -\arccos(-\frac{N}{\eta}) - \omega & \text{for} \quad \omega - \alpha N < 0, \end{cases} \tag{17}$$

and then plug in the saddle-node condition (15). In Fig. 1, we have plotted the saddle-node condition

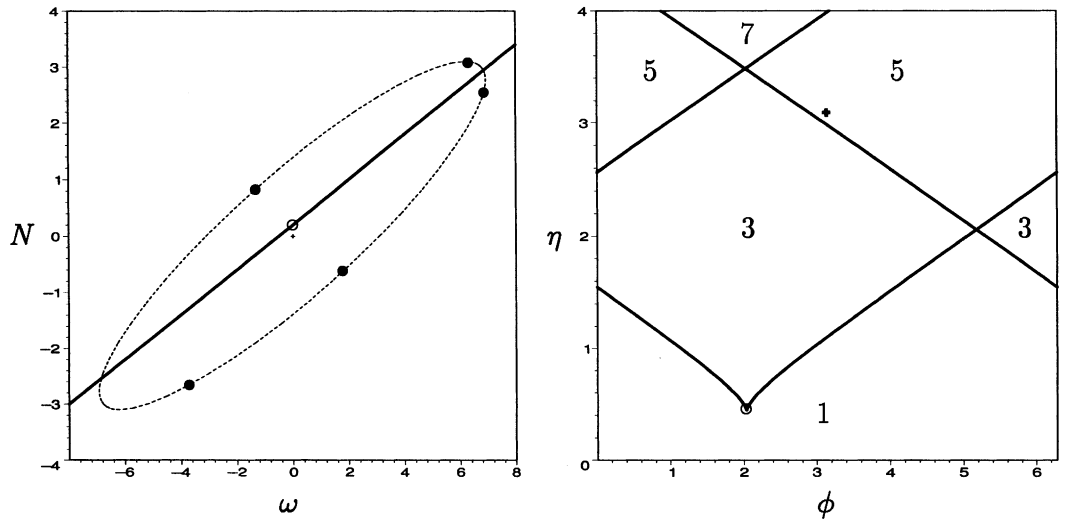

Fig. 1. Saddle-node curve with cusp-point (circle) for $\alpha = 2$. Left: (ω, N)-plane, ellipse for $\eta = 3.1$ with 5 ECMs for $\phi = \pi$. Right: (ϕ, η)-plane, number of ECMs.

(15) for fixed $\alpha = 2$, and the resulting curve in the parameter plane (compare [1]). Note that this curve has a singular point (called *cusp point*) which corresponds to a triple root of (12). Its location in the (ω, N)-plane can be computed as

$$\omega_s = 0, \quad N_s = \frac{1}{1+\alpha^2}, \tag{18}$$

and in parameter space

$$\eta = \frac{1}{\sqrt{1+\alpha^2}}, \quad \phi = (2k+1)\pi - \arctan(\alpha). \tag{19}$$

This value of η is the minimal feedback which is necessary to have under an appropriate phase condition more than one ECM on the ellipse.

The phase ϕ is only determined up to addition of multiples of 2π; looking at the interval $\phi \in [0, 2\pi]$, any bifurcation curve which leaves this interval at one side enters at the same time at the other side. At each branch of the saddle-node curve the number of solutions changes by two, leading to more and more ECMs for increasing η (see Fig. 1). The situation with five ECMs on the ellipse, given in the left part of the figure corresponds to the parameter values, indicated by the cross in the right-hand side of the figure.

2.2. The Petermann–Tager condition

It was first observed by Petermann and Tager in [8] that the existence of two ECM with the same carrier density may lead to stable pulsations of the laser with a frequency, given by the difference of the two ECM frequencies. These numerical observations were confirmed by results of Erneux e.a., showing by asymptotic expansion techniques [11] and later also with numerical path-following techniques [9,10] the existence of such pulsating solutions and corresponding Hopf bifurcations.

Here, we first want to derive an explicit condition for the existence of two ECMs with equal N. This can be done again using only the optical equation (3). We start with two copies of Eqs. (10) and (11)

$$N_{1,2} = -\eta\cos(\phi + \omega_{1,2}), \tag{20}$$

$$\omega_{1,2} - \alpha N_{1,2} = -\eta\sin(\phi + \omega_{1,2}). \tag{21}$$

Assuming $N := N_1 = N_2$ and $\omega_1 \neq \omega_2$, equations (20) give

$$\omega_1 + \phi = 2k\pi - (\omega_2 + \phi). \tag{22}$$

Adding now the two equations (21) yield

$$\frac{\omega_1 + \omega_2}{2} = \alpha N \quad \text{or} \quad \frac{\omega_1 - \omega_2}{2} = \omega_1 - \alpha N. \tag{23}$$

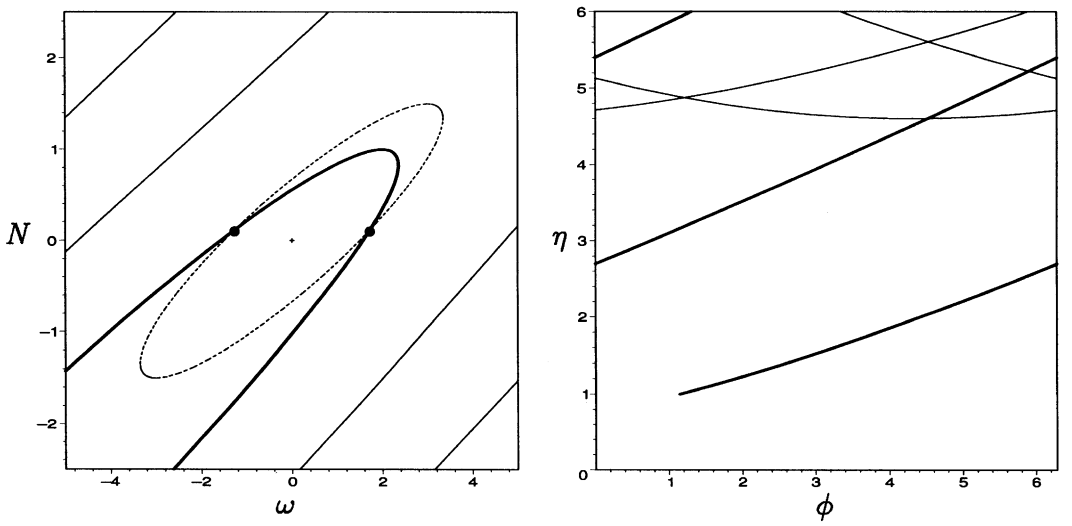

Fig. 2. Petermann–Tager condition (25) for $\alpha = 2$. Left: (ω, N)-plane; an arbitrary ECM ellipse for $\eta > 1$ intersects the curve at two ECM solutions with equal N. Right: (ϕ, η)-plane; due to the periodicity of ϕ the first (thick line) and second branch (thin line) appear repeatedly in the interval $\phi \in [0, 2\pi]$.

Inserting the relation (22) gives

$$\phi = k\pi - \alpha N. \tag{24}$$

Since we excluded the case $\omega_1 = \omega_2$, corresponding to $\omega_1 - \alpha N = 0$ (see (23)), we may divide (20) by (21) to eliminate η, giving finally

$$N = (\omega_1 - \alpha N)\cot(\omega_1 - \alpha N). \tag{25}$$

In Fig. 2, we have plotted the resulting curve for $\alpha = 2$ in the (ω, N)-plane and, using again (16), (17), also in the (ϕ, η)-plane of our primary bifurcation parameters. According to (25), a variation of the parameter α does not change the picture qualitatively. At the intersection points of the different solution branches in the parameter plane, we have two coexisting pairs of PT modes. However, the picture in the (ω, N)-plane indicates that the pair from the first branch should have the lowest threshold density. On the other hand, the existence of a stable pulsating solution can be expected only, if one mode of the PT pair is stable.

2.3. Mode degeneracy

Writing condition (9) for rotating wave solutions as

$$\lambda = (1 + \mathrm{i}\alpha)N_s + \eta \mathrm{e}^{-\mathrm{i}\phi}\mathrm{e}^{-\lambda} \tag{26}$$

with a complex spectral parameter λ instead of ω_s, we obtain the characteristic equation for the linear delay differential equation (3), depending parametrically on N. Hence, the ECM frequencies ω_s are eigenvalues λ which are purely imaginary. An optical mode degeneracy occurs, if there is a double eigenvalue, i.e., a double root of (26). Differentiating (26) by λ, we obtain

$$1 = -\eta \mathrm{e}^{-\mathrm{i}\phi}\mathrm{e}^{-\lambda}.$$

Together with (26) this has the unique solution $\lambda = (1 + \mathrm{i}\alpha)N - 1$, which is purely imaginary only if $N = 1$, giving $\lambda = \mathrm{i}\omega_s = \mathrm{i}\alpha$. This point with a degenerate ECM solution plays an important role for the dynamics of the system. Note that the saddle-node condition (15) is satisfied there. Also the first branch of the PT curve limits to this point, indicating that two ECM with equal N_s merge in the degeneracy point with the frequency difference going to zero. Correspondingly, there is a point of tangency of the ECM ellipse for $\eta = 1$ and the PT curve (see left part of Fig. 3).

There are further intersections between the PT curve and the saddle-node curve. They are not accompanied by a mode degeneracy, but may also

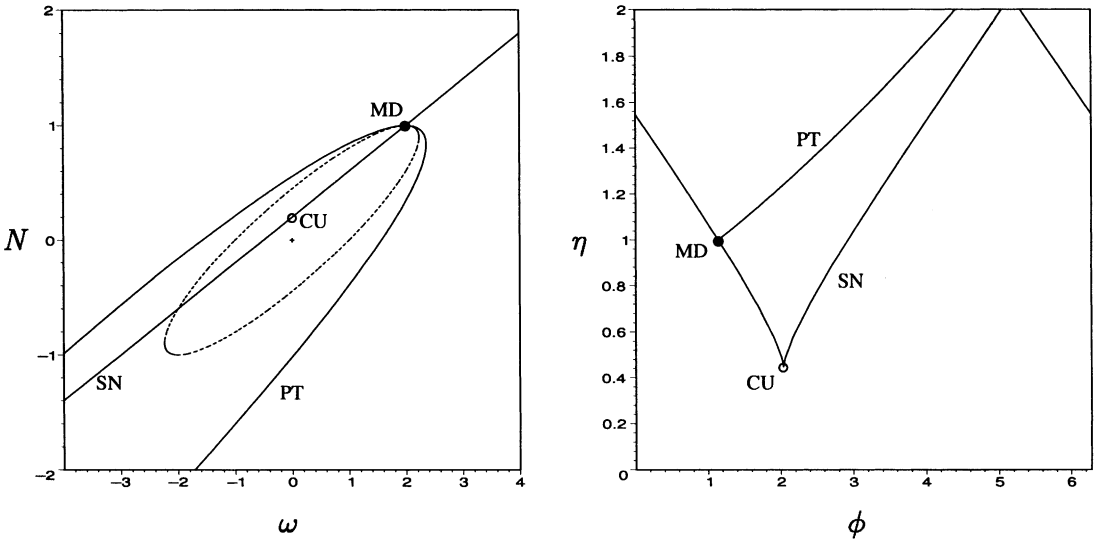

Fig. 3. Petermann–Tager (PT) and saddle-node bifurcation (SN) curves, mode degeneracy (MD) and cusp-point (CU) in the (ω, N)-plane (left) and in the (ϕ, η)-plane (right).

lead to interesting bifurcations. However, since they occur at much higher feedback levels, we will not study them here.

3. Linearized dynamics at external cavity modes

After having obtained a lot of information from the optical equation (3), we proceed in our stability and bifurcation analysis of the external cavity modes by considering the full system, including the carrier equation (4). For the theoretical background of our treatment of nonlinear differential delay systems we refer to [17,18].

First, we use a particular ECM solution

$$E(t) = E_s e^{i\omega_s t}, \quad N(t) = N_s, \tag{27}$$

where ω_s, N_s, E_s satisfy the ECM conditions (9), as a reference frame, introducing

$$E_{new}(t) := e^{-i\omega_s t} E(t).$$

The rotating wave solution (27) then becomes a stationary state of the transformed system

$$\dot{E}_{new}(t) = ((1 + i\alpha)N - i\omega_s) \cdot E_{new}(t) + \eta e^{-i(\phi+\omega_s)} \cdot E_{new}(t-1), \tag{28}$$

$$\dot{N}(t) = \varepsilon(J - N - (N + v)|E_{new}(t)|^2). \tag{29}$$

Splitting the equation for the optical field amplitude into real and imaginary part as $E_{new}(t) = x(t) + iy(t)$, we obtain

$$\begin{aligned}
\dot{x}(t) &= (x(t) - \alpha y(t))N + \omega_s y(t) \\
&\quad + \eta[x(t-1)\cos(\phi + \omega_s) + y(t-1) \\
&\quad \times \sin(\phi + \omega_s)], \\
\dot{y}(t) &= (\alpha x(t) - y(t))N - \omega_s x(t) \\
&\quad + \eta[y(t-1)\cos(\phi + \omega_s) - x(t-1) \\
&\quad \times \sin(\phi + \omega_s)], \\
\dot{N}(t) &= \varepsilon(J - N - (N + v)(x(t)^2 + y(t)^2).
\end{aligned}$$

This system can now be linearized in the form

$$\frac{d}{dt}\vec{v}(t) = A\vec{v}(t) + B\vec{v}(t-1)$$

with $\vec{v} = (v_1, v_2, v_3)$ corresponding to variation of x, y and N, respectively. The matrices A and B can be computed as

$$A = \begin{pmatrix} N & \omega_s - \alpha N & x - \alpha y \\ -(\omega_s - \alpha N) & N & \alpha x + y \\ -2\varepsilon x(N+v) & -2\varepsilon y(N+v) & -\varepsilon(1 + x^2 + y^2) \end{pmatrix}, \tag{30}$$

$$B = \begin{pmatrix} \eta\cos(\phi+\omega_s) & \eta\sin(\phi+\omega_s) & 0 \\ -\eta\sin(\phi+\omega_s) & \eta\cos(\phi+\omega_s) & 0 \\ 0 & 0 & 0 \end{pmatrix}. \tag{31}$$

The characteristic equation for the eigenvalues of this linear system is now given by the transcendental equation

$$\begin{aligned}\chi(\Lambda) &= \det(\Lambda\,\mathrm{Id} - A - \mathrm{e}^{-\Lambda}B) \\ &= \Big[(\Lambda - N - \mathrm{e}^{-\Lambda}\eta\cos(\phi+\omega_s))^2 \\ &\quad + (\omega_s - \alpha N + \mathrm{e}^{-\Lambda}\eta\sin(\phi+\omega_s))^2\Big] \\ &\quad \times (\Lambda + \varepsilon(1+x^2+y^2)) + 2\varepsilon(x^2+y^2)(N+v) \\ &\quad \times \big[\Lambda - (1+\alpha^2)N + \alpha\omega_s \\ &\quad + \mathrm{e}^{-\Lambda}\eta(\alpha\sin(\phi+\omega_s) - \cos(\phi+\omega_s))\big]\end{aligned}$$

with complex spectral parameter Λ. Using the ECM conditions

$$|E_s|^2 = x^2+y^2, \quad N = N_s = -\eta\cos(\phi+\omega_s),$$
$$\omega_s - \alpha N_s = -\eta\sin(\phi+\omega_s)$$

we obtain the characteristic equation for the linearization at the ECM solution as

$$\begin{aligned}\chi(\Lambda) &= \Big[(\Lambda + N_s(\mathrm{e}^{-\Lambda}-1))^2 \\ &\quad + (\omega_s - \alpha N_s)^2(\mathrm{e}^{-\Lambda}-1)^2\Big](\Lambda + \varepsilon(1+|E_s|^2)) \\ &\quad + \big[\Lambda + ((1+\alpha^2)N_s - \alpha\omega_s)(\mathrm{e}^{-\Lambda}-1)\big] \\ &\quad \times 2\varepsilon|E_s|^2(N_s+v).\end{aligned} \tag{32}$$

3.1. The Hopf condition

For a Hopf bifurcation it is necessary to have pair of pure imaginary solutions to (32), i.e.,

$$\chi(\Lambda) = 0, \quad \Lambda = i\Omega, \ \ \Omega \in \mathbf{R}.$$

The resulting equation can again be split into real part

$$\begin{aligned}0 &= 2\Omega(\cos\Omega - 1)\Big[\sin\Omega(N_s^2 + (\omega_s - \alpha N_s)^2) \\ &\quad - \Omega N_s\Big] + \varepsilon(1+|E_s|^2)\Big[-\Omega^2 \\ &\quad + 2\cos\Omega(\cos\Omega - 1)(N_s^2 + (\omega_s - \alpha N_s)^2) \\ &\quad + 2N_s\Omega\sin\Omega\Big] + 2\varepsilon|E_s|^2(N_s+v) \\ &\quad \times ((1+\alpha^2)N_s - \alpha\omega_s)(\cos\Omega - 1)\end{aligned} \tag{33}$$

and imaginary part

$$\begin{aligned}0 &= \Omega\Big[-\Omega^2 + 2\cos\Omega(\cos\Omega - 1)(N_s^2 + (\omega_s \\ &\quad - \alpha N_s)^2) + 2N_s\Omega\sin\Omega\Big] - 2\varepsilon(1+|E_s|^2) \\ &\quad \times (\cos\Omega - 1)\Big[\sin\Omega(N_s^2 + (\omega_s - \alpha N_s)^2) \\ &\quad - \Omega N_s\Big] + 2\varepsilon|E_s|^2(N_s+v) \\ &\quad \times (\Omega - ((1+\alpha^2)N_s - \alpha\omega_s)\sin\Omega).\end{aligned} \tag{34}$$

Due to the phase shift invariance of the rotating waves, $\Lambda = 0$ always solves the eigenvalue equation (32). Moreover, $\Lambda = 0$ is a double solution to (32) exactly at the saddle node curve (15). Exactly in these cases, $\Omega = 0$ is a solution to Eqs. (33) and (34).

3.2. Approximate solutions by scaling methods

In order to find approximating expressions for solutions of (33), (34), we use the smallness of ε. Assuming that there are solutions where $\Omega \neq 0$ stays away from zero as ε tends to zero, we can neglect terms of order ε in (33), (34). From the remaining terms

$$\begin{aligned}0 &= \sin\Omega(N_s^2 + (\omega_s - \alpha N_s)^2) - \Omega N_s, \\ 0 &= -\Omega^2 + 2\cos\Omega(\cos\Omega - 1) \\ &\quad \times (N_s^2 + (\omega_s - \alpha N_s)^2) + 2N_s\Omega\sin\Omega,\end{aligned} \tag{35}$$

we obtain the three conditions

$$N_s = -\frac{\Omega\sin\Omega}{2(\cos\Omega - 1)}, \tag{36}$$

$$\omega_s - \alpha N_s = \frac{\Omega}{2}, \tag{37}$$

$$N_s = (\omega_s - \alpha N_s)\cot(\omega_s - \alpha N_s). \tag{38}$$

This result coincides with Eq. (25) for the Petermann–Tager condition, i.e., for the existence of two ECM solutions with the same threshold value. Moreover, the Hopf frequency Ω coincides with the difference of the two ECM frequencies (compare (37) and (23)). For a more detailed analysis of these solutions, see [11,12].

Fig. 2 shows the curve, given by (38), which consists of several branches. Using Eqs. (16) and

(17), we obtain the corresponding curve in the (ϕ,η)-plane of our bifurcation parameters.

Note that the two branches of solutions to (38) which emanate from the point of mode degeneracy in the (ω,N)-plane, are mapped to the same branch in the (ϕ,η)-plane. Later we will see that solving numerically the full system (33) and (34), this coincidence will disappear, and two Hopf branches both close to this approximate curve will appear. This coincides also with the results in [9], where for changing η corresponding pairs of Hopf points have been found near the PT condition.

But in addition to these already known type of solutions, we get another type of solutions to (33) and (34), if we assume that Ω^2/ε remains finite for ε tending to zero (compare [15]). Here we may replace trigonometric functions by Taylor expansions and obtain for the rescaled variable

$$\Omega_{\mathrm{r}}=\frac{\Omega}{\sqrt{\varepsilon}}$$

in leading order of ε the equations

$$\begin{aligned}0 &= \Omega_{\mathrm{r}}^2(N_{\mathrm{s}}-N_{\mathrm{s}}^2-(\omega_{\mathrm{s}}-\alpha N_{\mathrm{s}})^2)-(1+|E_{\mathrm{s}}|^2)\\ &\quad\times((N_{\mathrm{s}}-1)^2+(\omega_{\mathrm{s}}-\alpha N_{\mathrm{s}})^2)-|E_{\mathrm{s}}|^2(N_{\mathrm{s}}+v)\\ &\quad\times((1+\alpha^2)N_{\mathrm{s}}-\alpha\omega_{\mathrm{s}}),\\ 0 &= -\Omega_{\mathrm{r}}^2((N_{\mathrm{s}}-1)^2+(\omega_{\mathrm{s}}-\alpha N_{\mathrm{s}})^2)+2|E_{\mathrm{s}}|^2(N_{\mathrm{s}}+v)\\ &\quad+(1-N_{\mathrm{s}}+\alpha(\omega_{\mathrm{s}}-\alpha N_{\mathrm{s}})).\end{aligned}$$

Eliminating Ω_{r}^2, and using the new coordinates

$$\bar{n}=1-N_{\mathrm{s}},\quad \bar{\omega}=\omega_{\mathrm{s}}-\alpha N_{\mathrm{s}}, \tag{39}$$

we get the Hopf condition

$$-\frac{1}{|E_{\mathrm{s}}|^2}=1+(1-\bar{n}+v)\left(\frac{\bar{n}+\alpha\bar{\omega}}{\bar{n}^2+\bar{\omega}^2}-\frac{(\bar{n}+\alpha\bar{\omega})^2-(1+\alpha^2)\bar{\omega}^2}{(\bar{n}^2+\bar{\omega}^2)^2}\right). \tag{40}$$

The corresponding Hopf frequency is given by

$$\Omega^2=\varepsilon\frac{2|E_{\mathrm{s}}|^2(N_{\mathrm{s}}+v)(\bar{n}+\alpha\bar{\omega})}{\bar{n}^2+\bar{\omega}^2}. \tag{41}$$

From this, we get the constraint $\bar{n}+\alpha\bar{\omega}>0$ in addition to the condition (40). Note that according to (41) the Hopf frequency along this branch of solutions is comparable to the relaxation frequency

$$\Omega^2\approx\Omega_{rel}^2=\varepsilon|E_{\mathrm{s}}|^2v$$

of the solitary laser. Hence we can interpret this branch of Hopf bifurcations as an undamping of the relaxation oscillation. The possibility of such pulsations has been pointed out already by Ritter and Haug in [7], performing a small signal analysis and introducing further simplifications. In the case of two-section DFB lasers, similar phenomena were called DQS-pulsations (dispersive self Q-switching), see [14]. In this case, obviously the Fabry–Perot dispersion of the external cavity leads to this type of instability.

Fig. 4 shows this DQS–Hopf curve together with the bifurcation curves, calculated before. Using Eq. (40), we obtain a bifurcation curve for fixed intensity $|E_{\mathrm{s}}|^2$. This means, the pumping parameter J has to be adjusted according to Eq. (13). Alternatively one could also use (13) to eliminate $|E_{\mathrm{s}}|^2$ in (40), and from that obtain a Hopf curve for constant J with varying intensity $|E_{\mathrm{s}}|^2$. In the figure we show the DQS–Hopf curve for several different choices of the intensity $|E_{\mathrm{s}}|^2$ and the parameter v (transparency level). Note that the dependence on these parameters originates from the carrier rate equation (4), which has not been used to calculate the conditions for saddle-node, PT, and mode degeneracy.

Note that all these Hopf curves start and end at the point of mode degeneracy

$$\bar{n}=\bar{\omega}=0.$$

However, both the finite Ω and $\Omega=\mathrm{O}(\sqrt{\varepsilon})$ approximations are no more valid in a neighbourhood of this point. To derive a correct approximation for the Hopf bifurcation curves near the mode degeneracy point, one should notice that near this point both the quantities Ω and ε/Ω^2 are small. Furthermore, closeness to the mode degeneracy point means that the quantities $\bar{n}$ and $\bar{\omega}$ are small as well. By expanding in powers of Ω, ε/Ω^2, $\bar{n}$ and $\bar{\omega}$, and omitting higher order terms, we obtain from Eq. (33) the approximate relation

$$\bar{n}-\bar{\omega}^2-\frac{\varepsilon}{\Omega^2}S(1+v)+\frac{\Omega^2}{6}\approx 0,$$

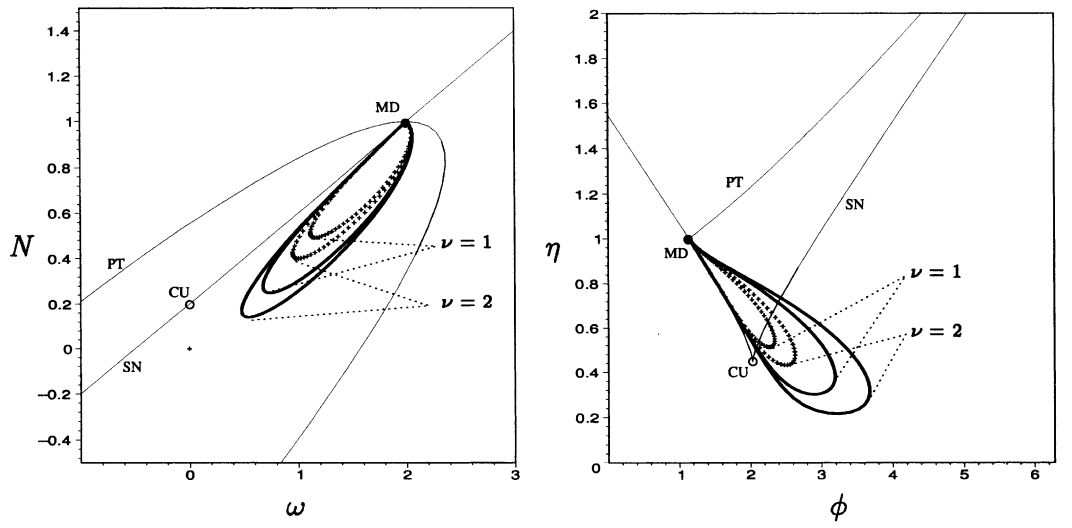

Fig. 4. Thick lines: bifurcation curves for the DQS–Hopf ($\alpha = 2$). Crosses: low intensity ($|E|^2 = 0.2$). Solid lines: high intensity ($|E|^2 = 2$).

and from (34) the approximate relation

$$\frac{\Omega^2}{4} - \bar{n}^2 - \bar{\omega}^2 + 2\frac{\varepsilon}{\Omega^2}S(1+v)(\alpha\bar{\omega} + \bar{n}) \approx 0.$$

To the leading order in Ω and ε/Ω^2 these equations give

$$\bar{n} \approx \frac{\varepsilon}{\Omega^2}S(1+v) + \frac{\Omega^2}{12},$$

$$\bar{\omega} \approx \alpha\frac{\varepsilon}{\Omega^2}S(1+v) \pm \sqrt{\left(\frac{\varepsilon}{\Omega^2}S(1+v)\right)^2(1+\alpha^2) + \frac{\Omega^2}{4}}.$$

Note that we have here two disjoint branches of the Hopf bifurcation curve. At small Ω and ε/Ω^2 we get small $\bar{n}$ and $\bar{\omega}$, i.e., these branches are indeed close to the mode degeneracy point ($N = 1$, $\omega = \alpha$). Each branch is parametrized by the value of Ω which runs monotonically from $O(\sqrt{\varepsilon})$ to small finite values, i.e., each branch asymptotically matches one of the ends of the DQS-type Hopf curve with one of the two Petermann–Tager curves.

It should also be noted that the "minus" branch intersects the saddle-node curve $\bar{\omega} = -\bar{n}/\alpha$ (cf. Eq. (15)). Indeed, the equation for the intersection point is

$$-\frac{\varepsilon}{\alpha\Omega^2}S(1+v) - \frac{\Omega^2}{12\alpha} \approx \alpha\frac{\varepsilon}{\Omega^2}S(1+v) - \sqrt{\left(\frac{\varepsilon}{\Omega^2}S(1+v)\right)^2(1+\alpha^2) + \frac{\Omega^2}{4}},$$

which gives indeed a unique solution

$$\Omega^3 \approx 2\varepsilon\frac{S(1+v)}{\alpha}\sqrt{1+\alpha^2}.$$

This intersection point (called "fold-Hopf interaction", or "Gavrilov-Guckenheimer point") is remarkable because its presence implies further nontrivial dynamics, such as bifurcation of invariant tori and homoclinic phenomena (see e.g. [19]). According to recent results in [20], a curve of torus bifurcation emanating from this point can be continued to the torus bifurcation, which has been found in [10]. However, on the torus branch close to the fold-Hopf interaction point, further bifurcations of 1:2 resonance were observed.

3.3. Numerical solutions for the Hopf condition

After having studied analytically the two types of Hopf bifurcations and their transition regime

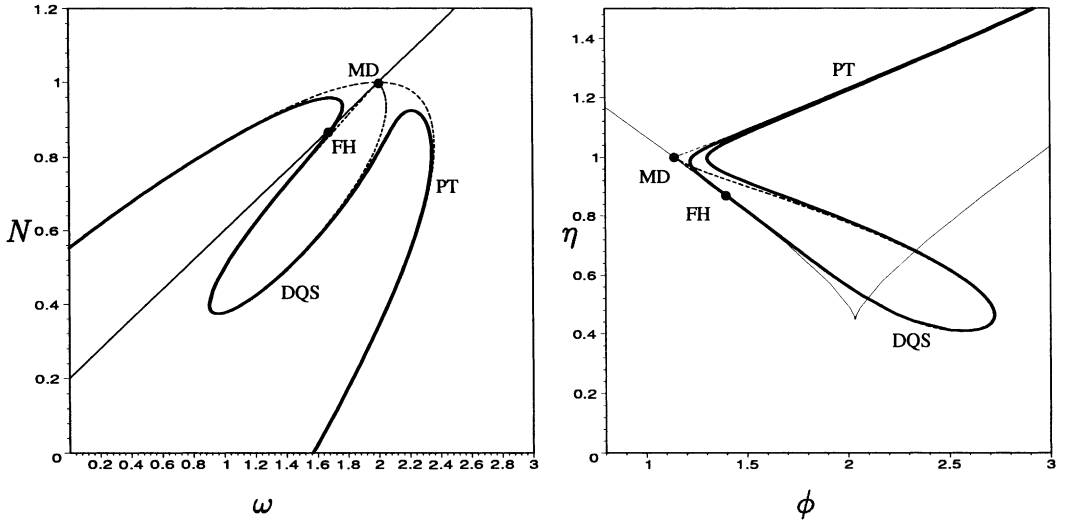

Fig. 5. Numerically obtained Hopf curves for $\varepsilon = 0.01$, $v = 1$, $|E|^2 = 0.5$ [left (ω, N)-plane, right: (η, ϕ)-plane]; dashed: curves from the asymptotic approximations (35), and (40); thin line: saddle-node curve; FH, fold-Hopf interaction.

near the point of mode degeneracy, we now present some numerical results: Fig. 5 shows a numerical solution to the system of equations (33), (34) for fixed values of the secondary parameters $\alpha, v, \varepsilon, |E|^2$. To make differences to the asymptotic curves (in the figure dashed) better visible, we have chosen $\varepsilon = 0.01$ only of moderate smallness. Apart from the point of mode degeneracy, the computed curve shows a good coincidence with the asymptotic PT and DQS curve.

Note that there are indeed two branches of the Hopf curve, both approaching the PT curve in the (ϕ, η)-plane. Each of them is connected with one of the two ends of the DQS curve. Moreover, one can see that in the vicinity of the mode degeneracy one branch of the Hopf curve meets the saddle-node line in a point of tangency (fold-Hopf interaction). Recall that in the (ω, N)-plane the region above the saddle-node line contains the ECM solutions of saddle type, whereas below the saddle-node line the nodes are located. This corresponds to the well known fact that at a fold-Hopf interaction point the type of the bifurcating equilibrium changes along the Hopf curve [19].

The organizing centre of the whole scenario is the point of optical mode degeneracy. It separates the two different regimes of DQS and PT pulsations, and leads to the nearby fold-Hopf interaction as well as to a second appearance of the Hopf curve in the vicinity of this point, where the frequency on this branch changes from order $\sqrt{\varepsilon}$ to order 1.

Since for the PT pulsation, the Hopf frequency is given by the beating frequency of the two modes, we can calculate explicitly the relation of this frequency Ω and the feedback level η: inserting (37) and (24) into (11), we obtain

$$\eta = \left| \frac{\Omega}{2 \sin(\Omega/2)} \right| \tag{42}$$

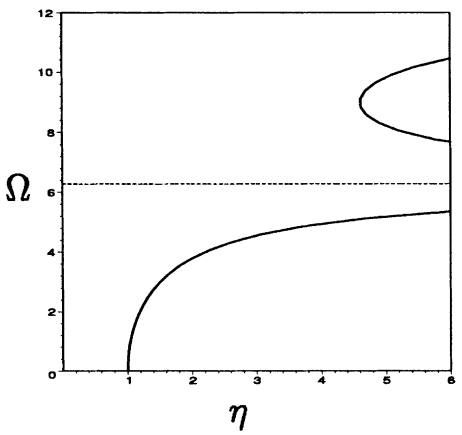

Fig. 6. PT Hopf frequency Ω for changing feedback level η, according to (42).

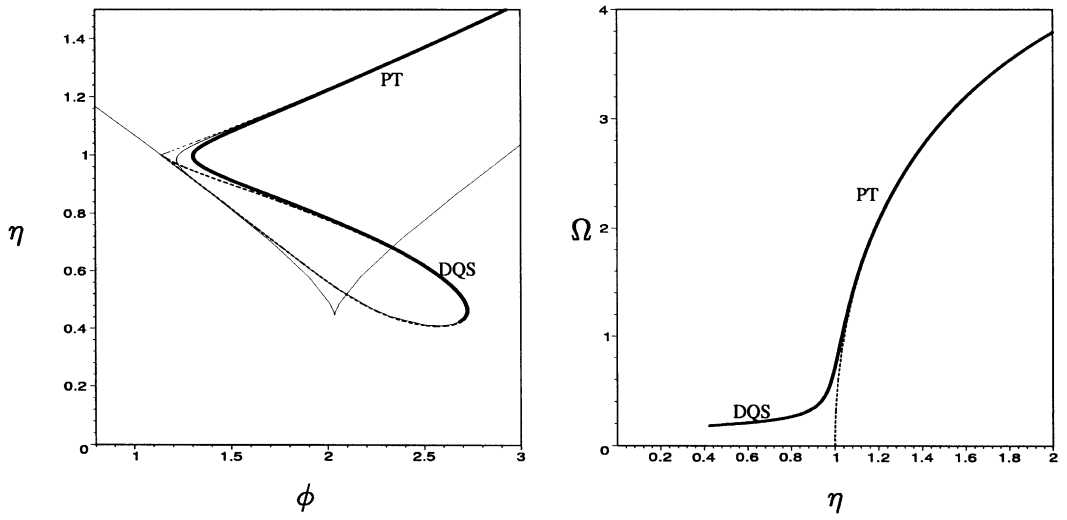

Fig. 7. Right: Hopf frequency Ω for changing feedback level η along the bold part of the Hopf curve in the bifurcation diagram (left). Dashed: asymptotic approximation for PT frequency, cf. Fig. 6.

Note that apart from the specific scaling of η and the time unit, there enters no specific parameter into this formula. Fig. 6 shows that the PT frequency on the first branch is tunable between zero and the value 2π in our rescaled time. However, it is necessary to meet the appropriate phase condition. For larger η there appear also more and more pairs of PT modes with larger frequency difference, the first of which leads to the second branch in Fig. 6.

In Fig. 7 we show the numerically obtained Hopf frequency along the part of the Hopf curve, connecting with increasing η the DQS and the PT regime. One can observe, that for $\eta < 1$ (i.e., the DQS case) the frequency is indeed of order $\sqrt{\varepsilon}$. Then, after an intermediate regime around $\eta = 1$, the curve follows the curve given by (42).

4. Conclusions

We have studied Hopf bifurcations, leading to pulsation instability of lasers with optical feedback. Restricting to the case of moderate feedback time, as it occurs in integrated multi-section devices, we obtain a complete characterization of solutions to the bifurcation equation and a two-dimensional bifurcation diagram in the main parameters feedback strength η and feedback phase ϕ.

Depending on the pulsation frequency, one can distinguish two different types of pulsations, the DQS- and Petermann–Tager (PT) pulsations. The frequency of the first type is related to the relaxation frequency of the solitary laser, whereas for the second type it is determined by the frequency difference of two external cavity modes with the same threshold density, leading to higher frequencies. The occurrence of these two types of pulsations is separated by a distinguished feedback level (in our rescaled variables $\eta = 1$). Using the ratio of feedback time and carrier lifetime as a small parameter, we were able to compute approximating expressions for the bifurcation curves in the different regimes, showing also the influence of secondary parameters. We also compared these approximating formulas with numerical solutions to the full problem.

Finally, we studied the transition between the two types, which is organised by a point of mode degeneracy and comes along with a codimension-two bifurcation of Guckenheimer–Gavrilov type (fold-Hopf interaction). This codimension two bifurcation is known to give rise to complicated dynamics and nonlocal bifurcations.

The two presented mechanisms for pulsations seem to be fundamental for laser devices where a moderately delayed feedback is present. Especially the role of the point of mode degeneracy as an organizing centre for the different types of pulsations seems to be a more general feature [15]. Indeed, similar bifurcation scenarios have been obtained in [20] for three-section lasers with one active section. These results, however, are based on a time domain model, and have been obtained by centre manifold techniques and numerical path-folloiving of bifurcation curves.

The high frequency pulsations of the PT type (for appropriate device parameters more than 40 GHz should be possible), together with the shown tunability of their frequency seem to be a promising feature for applications in optical communication technique.

References

[1] G.H.M. van Tartwijk, G.P. Agrawal, Prog. Quantum Electron. 22 (1998) 43.
[2] R.L. Davidchack, Y.-C. Lai, A. Gavrielides, V. Kovanis, Physica D 145 (2000) 130.
[3] T. Heil, I. Fischer, W. Elsäßer, Phys. Rev. A 58 (4) (1998) R2672.
[4] T. Heil, I. Fischer, W. Elsäßler, A. Gavrielides, Phys. Rev. Lett. 87 (24) (2001) 243901.
[5] B. Tromborg, J.H. Osmundsen, H. Olesen, IEEE J. Quantum Electron. 20 (9) (1984) 1023.
[6] J. Mørk, B. Tromborg, J. Mark, IEEE J. Quantum Electron. 28 (1) (1992) 93.
[7] A. Ritter, H. Haug, J. Opt. Soc. Am. B 10 (1) (1993) 130.
[8] A.A. Tager, K. Petermann, IEEE J. Quantum Electron. 30 (7) (1994) 1553.
[9] D. Pieroux, T. Erneux, B. Haegeman, K. Engelborghs, D. Roose, Phys. Rev. Lett. 87 (19) (2001) 193901.
[10] D. Pieroux, T. Erneux, T. Luzyanina, K. Engelborghs, D. Roose, Phys. Rev. E 63 (3) (2001) 036211.
[11] T. Erneux, F. Rogister, A. Gavrielides, V. Kovanis, Opt. Commun. 183 (2000) 476.
[12] T. Erneux, in: R.H. Binder, P. Blood, M. Osinski (Eds.), Physics and Simulation of Optoelectronic Devices VIII, Proc. SPIE, vol. 3944, 2000, p. 588.
[13] M. Radziunas, H.-J. Wünsche, D. Sartorius, O. Brox, D. Hoffmann, K. Schneider, D. Marcenac, IEEE J. Quantum Electron. 36 (9) (2000) 1026.
[14] U. Bandelow, H.-J. Wünsche, B. Sartorius, M. Möhrle, IEEE J. Select. Top. Quantum Electron. 3 (1997) 270.
[15] D. Turaev, Fundamental obstacles to self-pulsations in low-intensity lasers, WIAS-Preprint No. 629, 2001.
[16] R. Lang, K. Kobayashi, IEEE J. Quantum Electron. 16 (1980) 347.
[17] J.K. Hale, S.M. Verduyn Lunel, Introduction to Functional Differential Equations, Appl. Math. Sci., vol. 99, Springer, New York, 1993.
[18] S.M. Verduyn Lunel, B. Krauskopf, in: AIP Conf. Proc., vol. 548, 2000.
[19] Y.A. Kusnetsov, Appl. Math. Sci. 112 (1995).
[20] J. Sieber, Numerical bifurcation analysis for multi-section semiconductor lasers, WIAS-Preprint No. 683, Berlin, 2001.